

Molecular Design beyond Training Data with Novel Extended Objective Functionals of Generative AI Models Driven by Quantum Annealing Computer

Hayato Kunugi¹, Mohsen Rahmani², Yosuke Iyama¹, Yutaro Hirono¹, Akira Suma¹, Matthew Woolway², Vladimir Vargas-Calderón², William Kim², Kevin Chern², Mohammad Amin², and Masaru Tateno^{1*}

1 Innovation to Implementation Laboratories, Central Pharmaceutical Research Institute,
Japan Tobacco Inc., Takatsuki, Osaka 569-1125, Japan

2 D-Wave Systems Inc., 3033 Beta Ave, Burnaby, BC V5G 4M9, Canada

* Corresponding should be addressed. Email: masaru.tateno@shionogi.co.jp

Abstract

Deep generative modeling to stochastically design small molecules is an emerging technology for accelerating drug discovery and development. However, one major issue in molecular generative models is their lower frequency of drug-like compounds. To resolve this problem, we developed a novel framework for optimization of deep generative models integrated with a D-Wave quantum annealing computer, where our Neural Hash Function (NHF) presented herein is used both as the regularization and binarization schemes simultaneously, of which the latter is for transformation between continuous and discrete signals of the classical and quantum neural networks, respectively, in the error evaluation (*i.e.*, objective) function. The compounds generated via the quantum-annealing generative models exhibited higher quality in both validity and drug-likeness than those generated via the fully-classical models, and was further indicated to exceed even the training data in terms of drug-likeness features, without any restraints and conditions to deliberately induce such an optimization. These results indicated an advantage of quantum annealing to aim at a stochastic generator integrated with our novel neural network architectures, for the extended performance of feature space sampling and extraction of characteristic features in drug design.

(186 words)

Introduction

In the field of drug discovery, efficiently designing molecular structures with optimal chemical properties and synthetic accessibility is a complex and important research area. Typical approaches such as iterating through the design and experiment cycle can only search a small region in a vast chemical space, where the number of synthesizable molecules of size acceptable for drugs is estimated to be over 10^{60} ¹. Machine learning and deep learning-based drug design can efficiently explore a wider region in such a huge chemical space. Actually, by applying recent achievements in deep learning and deep generative models, various deep generative models have been reported for molecules with desired chemical properties^{2,3}.

Despite these efforts, two challenges with compounds generated from existing generative models remain: 1) the low frequency of “drug-like” molecules that satisfy the activity to the target proteins and have acceptable chemical properties and synthetic accessibility; and 2) a trade-off between the character of the compounds and the diversity in the chemical structure⁴. One cause of these problems is the lack of data, resulting in low generalization due to overfitting. Currently, the number of compounds that can be synthesized is $\sim 10^{10}$ ⁵, whereas the expected size of the chemical space is 10^{60} (as previously mentioned)—thus, the number of synthesizable compounds represents only a very small proportion of the entire chemical search space, and is insufficient for use as training data.

Quantum machine learning (QML) (also referred to as quantum artificial intelligence (QAI)) is a growing area of research that combines quantum computing and machine learning. QML investigates how quantum resources such as superposition, entanglement, and tunneling can accelerate or enhance classical learning models. Most early work has focused on the gate-based paradigm, where data and model parameters are encoded into quantum circuits composed of unitary transformations and projective measurements. Algorithms such as quantum support vector machines, kernel estimators, and quantum neural networks are

implemented through parameterized quantum circuits, optimized using hybrid quantum-classical feedback loops⁶. However, in many common scenarios, training parameterized quantum circuits has been shown to be unlikely to be able to scale due to trainability issues known as barren plateaus⁷; it may also be possible for classical computing to efficiently simulate such quantum circuits⁸.

An alternative and more physically motivated framework arises in quantum annealing^{9,10}, which provides an analog realization of optimization and sampling tasks central to machine learning. In quantum annealing, learning problems are mapped onto an Ising Hamiltonian and the system searches for the low-energy configurations. Sampling from these configurations can be guided by training the parameters of the Ising Hamiltonian to learn a “binary” data distribution or a “binary” latent representation of an autoencoder. Quantum annealers, such as D-Wave’s Advantage2TM quantum computer, implement these dynamics in hardware, enabling large-scale exploration of complex energy landscapes for machine learning applications^{11–13}. Recent experiments have demonstrated that quantum annealing achieves a scaling advantage in approaching low-energy configurations^{14,15}, while the resulting sampling distributions cannot be efficiently reproduced by any known classical simulation¹⁵. Therefore, it is important to explore ways to harness this intrinsic sampling power for quantum-enhanced generative modeling in areas such as drug discovery and materials design.

In this report, our approach started from Variational Autoencoder (VAE)-based generative models for generation and inference of chemical compounds. VAE sets the approximated posterior distribution of the latent variables and optimizes the evidence lower bound (ELBO) instead of the true log-likelihood, which is generally intractable. By the amortized inference and the reparameterization framework^{16,17}, VAE can efficiently train its objective function, which is also referred to as the loss function with the reconstruction loss

and regularization terms included, and is widely used for the generative model. TransVAE³ also involves the VAE that generates character sequences of molecules via a combination of Transformer-based Encoder/Decoder and continuous-valued latent space. More recently, VAE with discrete latent variables, Discrete VAE (DVAE)¹⁸, in which the generative process is driven by a Boltzmann Machine (BM), was adopted for the generation of chemical compounds¹⁹.

DVAE incorporates discrete latent variables with a discrete prior, making it a more suitable alternative for modeling data with categorical structures such as molecular descriptors tokenized by employing a particular transformation scheme. In addition, DVAE is suitable for combining a VAE architecture with quantum computing in which measurement outcomes are binary (spin) states. Quantum VAE²⁰ replaced the prior distribution from a classical BM with a quantum Boltzmann machine (QBM)²¹ in which the D-Wave quantum annealer leveraged the sampling from the Boltzmann distribution.

In DVAE, converting a continuous representation of the input data to a binary representation in the final encoding step, is not differentiable and, thus, prevents gradients of the error (reconstruction loss) from being backpropagated to the encoder. To solve this issue, DVAE introduced auxiliary continuous variables for training the approximating posterior, which stochastically converted from the discrete variables^{18,22}. Considering a specific form of the smoothing distribution, the error can be propagated back through the latent variables by reparameterization. During training, only discrete variables are used in the prior distribution, whereas continuous variables are used in the approximating posterior. Thus, non-differentiability for backpropagation is still a crucial issue in this scheme.

We propose another approach to solve the non-differentiability of the encoder by involving our novel scheme in the objective function of the autoencoder-based generative model. In this scheme, inspired by Deep Hashing²³, the output of the encoder is binarized

using outputs of a “deterministic” function (*i.e.*, a stochastic distribution is not involved) as the latent variables. An additional term that aims to reduce the loss in binarization is included in the total objective (loss) function for error evaluation of the system. Carefully defining the structure of the loss function and its derivatives enables the loss to backpropagate through the latent variables without smoothing and stochastic reparameterization (differentiability). We applied this scheme to our generative models of chemical compounds, thereby showing that employment of this scheme improved the validity and drug-likeness of the generated compounds in both classical and quantum computations of the prior distributions.

In addition, we utilized QBM as a prior distribution of the compound generation model, thus indicating that the quantum prior outperforms the classical counterpart in the quality of the generated compounds. Interestingly, the compounds generated via our “quantum” generative model exhibited a higher quality in both structural validity and drug-likeness scores than those of even the training dataset without any conditions to deliberately induce optimal trends of the evaluation scores. Thus, our present analysis suggests that our novel objective functionals integrated with the D-Wave quantum annealer should possess a powerful potential for the sampling task of the drug discovery field.

Results

Quantum Annealing

To solve the learning problems using quantum annealing, the Ising Hamiltonian is formulated as

$$H(s) = A(s) H_D + B(s) H_P$$

$$H_D = - \sum_i \sigma_i^x, \quad H_P = \sum_{i,j} J_{ij} \sigma_i^z \sigma_j^z + \sum_i h_i \sigma_i^z \quad (1)$$

where H_D is a transverse-field driver promoting quantum tunneling, H_P encodes the cost

function or model parameters and σ_i^x, σ_i^z are Pauli operators for i -th element. By slowly varying the annealing schedule $A(s)$ and $B(s)$, the system evolves toward the low-energy configurations of H_P . Sampling from these configurations can be guided by training the parameters J_{ij} and h_i to learn the prior distribution of binary latent variables (see Equation 2).

VAE and DVAE

The training framework of the original VAE is formulated by the variational inference, which maximizes ELBO on the true log-likelihood of data:

$$\mathcal{L} = \mathbb{E}_{q_\phi(z|x)}[\log p_\theta(x|z)] - D_{KL}(q_\phi(z|x) \parallel p_\psi(z)) \leq \log p_\theta(x), \quad (2)$$

where ϕ, θ , and ψ denote the trainable parameters for the encoder, decoder, and prior. The prior parameters ψ includes the parameters of Ising Hamiltonian J_{ij}, h_i (see Equation 1). The first term corresponds to the reconstruction loss which measures the expected log-likelihood (decoder) $p_\theta(x|z)$ of the data x given the latent variables z under the approximate posterior (encoder) $q_\phi(z|x)$. The second term represents the Kullback-Liebler (KL)-divergence between the approximated posterior $q_\phi(z|x)$ and the prior $p_\psi(z)$. The training objective is

$$\begin{aligned} \text{argmin}_{\phi, \theta, \psi} \mathbb{E}_{x \sim \mathcal{D}}[L_{elbo}(x; \phi, \theta, \psi)] \\ L_{elbo} := \underbrace{-\mathbb{E}_{q_\phi(z|x)}[\log p_\theta(x|z)]}_{L_{rec}(x; \phi, \theta)} + D_{KL}(q_\phi(z|x) \parallel p_\psi(z)) \end{aligned} \quad (3)$$

where \mathcal{D} denotes the data (empirical) distribution.

DVAE¹⁸ incorporates discrete latent variables with a discrete prior, making DVAE a better alternative for modeling data with categorical structures. Simplified Molecular Input

Line Entry System (SMILES)²⁴ and SELF-referencing Embedded Strings (SELFIES)²⁵ are widely used for encoding molecules to sequences of strings. We created molecular descriptors tokenized from SMILES strings. In addition, DVAE is suitable for combining the VAE architecture with quantum computing where the observed values are binary (spin) states.

DVAE proposed a stochastic binarization to characterize the posterior distribution $q_\phi(z|x)$ for D -dimensional discrete latent variables $z = (z_i)_{i=1,\dots,D} \in \{0, 1\}^D$ from outputs of the encoder $l = (l_i)$ as follows:

$$q_i = \sigma(l_i)$$

$$z_i = \mathcal{H}(q_i + \rho_i - 1) = \mathcal{H}(l_i + \sigma^{-1}(\rho_i)), \quad \rho_i \sim \text{Unif}(0, 1), \quad (4)$$

where $\sigma(x) = \frac{1}{1+e^{-x}}$, $\sigma^{-1}(y) = \log y - \log(1 - y)$ denotes the sigmoid function and its inverse, and \mathcal{H} denotes the Heaviside step function. The main obstacle of VAE with discrete latent variables is that the function $z = z_\phi(x, \rho)$ is non-differentiable such as Heaviside, which prevents backpropagation using the reparameterization trick. Gumbolt^{22,26} applied the Gumbel trick²⁷: a smoothing of z to obtain a continuous variable $\zeta = (\zeta_i)_{i=1,\dots,D} \in (0, 1)^D$ by $\zeta_i = \sigma\left(\frac{l_i + \sigma^{-1}(\rho_i)}{\tau}\right)$, where τ is a smoothing parameter with $\zeta \rightarrow z$ in the limit of $\tau \rightarrow 0$.

Involvement of the Neural Hash Function (NHF)

Herein, we aimed to solve the afore-mentioned, non-differentiable features derived from the binarization of discrete latent variables. We first constructed a Transformer²⁸-based encoder-decoder architecture with discrete latent variables.

Let $X \in \mathbb{N}^{N \times C}$ represent the tokenized SMILES of N molecules using a vocabulary size of V , where C denotes the maximum number of tokens. Each element $(X_{nc} \in \{1, 2, \dots, V\})$ of X represents the index of the c -th token of the n -th molecule. Tokens are

embedded in a d_{model} -dimensional space and fed into an encoder f_ϕ including Transformer layers, a Neural Tensor Network block, and MLP layers (see Methods) to obtain the D -dimension fixed length vectors $H = (h_1, h_2, \dots, h_N) \in \mathbb{R}^{N \times D}$. Binary latent variables $Z = (z_1, z_2, \dots, z_N) \in \{0,1\}^{N \times D}$ are obtained from H through a binarization function and fed into a decoder g_θ including another Neural Tensor Network and Transformer layers. Finally, outputs of the decoder are passed through a softmax layer to get probabilities of reconstructed tokens $\hat{X} \in \mathbb{R}^{N \times C \times V}$.

Inspired by Deep Hashing²³, we construct the loss function L_{nhf} , referred to here as the Neural Hash Function (NHF), as the objective (loss) function of our generative models (see Methods for details):

$$\begin{aligned}
L_{nhf} &= L_{rec}(X, \theta, \phi) + L_{prior}(\phi, \psi) + L_{quant}(X, \phi), \\
L_{rec} &:= \frac{1}{N} \sum_n CE(X_n, \hat{X}_n), \\
L_{prior} &:= -\frac{1}{N} \sum_n \log p_\psi(z_n), \\
L_{quant} &:= \frac{\lambda_{fro}}{2N} \|Z - H\|_F^2 + \frac{\lambda_{ortho}}{2} \sum_l \|W_l W_l^T - I\|_F^2,
\end{aligned} \tag{5}$$

where CE denotes the cross entropy and $\|\cdot\|_F$ denotes the Frobenius norm (L2-norm) defined for matrices. L_{rec} is the reconstruction loss as the cross entropy between inputs and reconstructed tokens. L_{prior} is the approximated cross entropy of the prior distribution $p_\psi(z)$ and the empirical distribution. L_{quant} means the quantization loss to produce good binary codes. The first term is the binarization loss to minimize the gap before and after the binarization. The second term encourages the weight matrices $W_l, l = 1, 2, \dots, L$ of the L -layer MLP in the encoder to be orthogonal, that is, requiring the different dimensions to be independent.

In Deep Hashing, the transformation from H to Z is performed by a non-smooth

function such as Heaviside function. To optimize the model parameters by the stochastic gradient descent method, we defined the gradient of L_{nhf} with respect to the parameters of the decoder θ , prior ψ , and encoder ϕ , as follows (see Methods for details):

$$\begin{aligned}\frac{\partial L_{nhf}}{\partial \theta} &= \frac{\partial L_{rec}(X; \phi, \theta)}{\partial \theta} \\ \frac{\partial L_{nhf}}{\partial \psi} &= \frac{\partial L_{prior}(Z; \phi, \psi)}{\partial \psi} \\ \frac{\partial L_{nhf}}{\partial \phi} &= \sum_{n=1}^N \delta_n^T \frac{\partial h_n}{\partial \phi} \\ \delta_n &:= \frac{\lambda_{fro}}{N} (z_n - h_n) + \frac{\partial L_{rec}(X; \phi, \theta)}{\partial z_n} + \frac{\partial L_{prior}(Z; \phi, \psi)}{\partial z_n}\end{aligned}\tag{6}$$

The scheme of the entire model and the workflow of the training and generation phase are shown in Figure 1.

We examined the effect of the molecular generation model using the NHF. This model inputs and outputs the SMILES sequences as representations of chemical structures. We trained the model using the ChEMBL public dataset, and generated the compounds from the BM prior and the Decoder. We evaluated the validity of the generated SMILES, a fraction of SMILES strings that were successfully converted into molecular structures, as a metric for generative models. Our NHF outperformed the validity of the Gumbel-Softmax binarization (52.2% in Gumbel-Softmax and 62.0% in NHF for the fully classical computations) (Table 1).

Employment of the quantum annealer for sampling latent variables from the prior

The major challenge in training BM is sampling from the model distribution. The Quantum Boltzmann Machine (QBM)²¹ is the learning scheme of the quantum Boltzmann distribution derived from a transverse field Ising Hamiltonian using the quantum annealing processor (see Equation 1). To the effect of QBM, we trained the generative model with QBM

or classical BM (see Methods). The loss of the QBM model converged within 300 epochs as the classical BM model did (Figure S3). As a consequence, the validity of compounds generated by QBM were higher than those from classical BM (97% in QBM and 73% in classical BM) (Table 1).

Next, we compared the distributions of molecular properties and drug-likeness score (QED score²⁹) from generated compounds. Surprisingly, compounds sampled from QBM shifted their distribution of the QED score towards the higher QED side. Moreover, the proportion of drug-like compounds (QED > 0.7) was higher than those from classical BM and even the training data (Table 2). This phenomenon was specific to QBM, while samples from classical BM simply reproduced the training data (Figure 2). It should be noted herein that the afore-mentioned, molecular generation beyond the training dataset in the quality related to the drug-likeness score was achieved without any inductions of the trends, such as some restraints and stochastic conditions.

Notably, under the QBM prior, the NHF-based model showed superior validity (Table 1) and drug-likeness (Figure 2, Table 2) compared to the Gumbel-Softmax-based model. Through the training steps, the coupling weights between the latent variables (spins) (see Equation 1) are optimized along with the other parameters. At the end of the training, the NHF-based model acquired denser spin-spin coupling than the Gumbel-Softmax-based model (Figure 3).

Subsequently, we compared relationships between transformation of chemical structures and improvement of the QED scores in the training data and samples generated by the QBM model (*i.e.*, the latter is referred to herein as the generated data). We picked up 42 representative compounds from the training data and collected a subset of compounds in the generated data, for which substructures were matched with those of the representative compounds in the training data. This subset of the generated data is further distinguishably

comprised of characteristic subsets using the following two similarity metrics: the Matching Coefficient (MC) of matched heavy atoms and the Tanimoto Similarity (TS) of the molecular fingerprints (see Methods for details) (Figure 4).

More specifically, in the scatter plot of the MC and TS (Figure 4), the region with high MC and low TS values ($MC > 0.5$ and $TS < 0.2$) includes the following compounds: the chemical structures significantly differ from the matched, original compounds in the training data, while the molecular sizes are comparable to them. For example, a chain group of the original compounds in the training data is converted into ring structures, which may thus lead to a type of “scaffold hopping” from the original compounds. Conversely, the region with low MC and high TS values ($MC < 0.5$ and $TS > 0.4$) contains compounds with their scaffold conserved as that of the matched, original compounds in the training data (“scaffold preserving”), although their side chains are modified. We calculated the difference of the QED score between the generated and original (matched) compounds in the generated and training data, respectively. As a consequence, we found that the high-MC and low-TS subsets (“scaffold hopping” subset) exhibited a higher proportion of compounds with improved QED, compared to the low-MC and high-TS subset (“scaffold preserving” subset) (Figure 4). This feature of our quantum computational system with the QBM prior and NHF-based loss function is very useful for drug design, since scaffold hopping is still actually an intractable task.

Adaptation of the NHF to an MLP-based architecture

To evaluate the scope of applicability of the NHF, we additionally performed the compound generation employing an MLP-based encoder-decoder architecture. Using a 3-layer encoder and decoder, the validity of the MLP-based model with the NHF (the NHF validity) was also superior to that of Gumbel-Softmax (the Gumbel-Softmax validity) (Table

3). Compared with the afore-mentioned, Transformer-based architecture, MLP-based architecture increased the uniqueness of generated molecules. Thus, with a modest reduction in validity, the number of unique compounds is comparable to that of the Transformer-based architecture. Note that the Gumbel-Softmax validity coupled with the QBM model was 38.0%, which means that the MLP architecture does not work without employing NHF as a molecular generation model.

Discussion

Role of the NHF in our objective functions (I): beyond VAE in posterior approximation

We developed a novel training scheme for autoencoder-based generative models in which the latent variables are converted from continuous to discrete by the NHF for integration with quantum annealing BM, as the prior. As a consequence, the performance related to the molecular generation definitively increased with respect to the two distinct types of the autoencoder architecture (*i.e.*, Transformer- and MLP-based autoencoders) which suggests that our NHF is a robust scheme applicable to a wide range of architectures.

Compared to the loss function of DVAE (*i.e.*, L_{elbo} (Equation 3)), the KL-divergence term is replaced with the binarization loss in the NHF (Equation 5), which thereby minimizes the gap between the binary and original (continuous) latent variable vectors. In this manner, a novel loss function is adopted in our present generative models. Although in DVAE, KL-divergence works as the regularization term, which makes the posterior distribution closer to the prior distribution (*i.e.*, posterior approximation), balancing both reconstruction error and regularization is difficult due to repulsive effects on the entire objective. Most proposed methods for alleviating the shortcomings of the conventional VAE scheme derived from KL-divergence³⁰⁻³² require careful tuning of hyperparameters. In contrast, our presented approach is simpler: remove the KL-divergence term and establish the

binarization of the latent variables, resulting in a constraint for the generative AI system (*i.e.*, requiring the conversion of discrete and continuous latent variables).

Role of the NHF in our objective functions (II): tractable differentiability

A further advantage of our NHF is found in a crucial issue for AI systems, which is related to the differentiability (*i.e.*, backpropagation). In our NHF scheme, the binarization loss is defined by the matrix norm for all samples in the minibatch (Equation 5), which is effective for approximating the gradient through the binarization function (Equation 6). This is consistent with the previous report in which the empirical loss gains smoothness as larger sample size, when the gradients are approximated by the Straight Through Estimator (STE)³³. Using the matrix norm can have another advantage: “aggregated posterior”³⁴. Since the conventional VAE models the posterior distribution using the mean-field approximation, that is, $q_\phi(z|x) = \prod_n q_\phi(z|x_n)$ in Equation 1, the objective (especially the KL-divergence term) independently forces each component $q_\phi(z|x_n)$ closer to the prior $p_\psi(z)$, which often becomes the low expressiveness of the latent variables (*i.e.*, posterior collapse)^{35,36}. In our NHF scheme, we consider the collection of the latent variables for the objective, which is equivalent to a comparison between the mixture of the posterior $\sum_n q_\phi(z|x_n)$ and the prior. Using our NHF scheme, the objective function stepped out of the framework of VAE and led to better performance for our generative models.

Role of the NHF in our objective functions (III): free from reparameterization in VAE

Comparing binarization schemes reveals another advantage of the NHF. In the typical VAE, the model distribution of the posterior is limited to the specific family for applying the reparameterization. To apply the reparameterization, we search for a distribution $q_\phi(z|x)$ that can be decomposed by the differentiable transformation $\xi_\phi(x, \rho)$ and auxiliary

variable $\rho \sim p(\rho)$. Herein, three approaches were suggested¹⁶ for the posterior distribution: (1) tractable and differentiable inverse cumulative distribution function (CDF); (2) computation employing a “standard” distribution and its shape parameters; and (3) their composition. Gaussian distribution is the simplest example used in almost all VAE cases. In the discrete cases, posterior distribution is modeled by a factorized Bernoulli distribution and Gumbel-Softmax (Equation 4) or the other variations using the sigmoid function for smoothing¹⁸. However, such treatments can cause the vanishing gradient. We showed that NHF models have denser connections between latent variables (Figure 3), suggesting that the NHF can pass the gradient more efficiently than smoothing-based methods. In this manner, our NHF scheme exhibits a great advantage in the training of the AI system through reducing the restriction of the distribution shapes found in VAE.

We trained our models using the same dataset as a published model with the conventional VAE¹⁹ in this report, and revealed that the validity of the generated compounds was improved (54% and 97% in the previous and present reports, respectively). Our NHF exhibits an appropriate affinity with QBM, which can produce the distribution distinguished from that produced by the classical BM (Figure 2). In fact, we showed that QBM models increased the population of drug-like compounds, even when compared to training datasets (Table 2). It should be noted herein that we used only the tokens representing compound’s chemical structures (SMILES) for training and did not provide any information concerning molecular properties for both training and generation processes of our generative models. The QBM model successfully generated more drug-like compounds, as if the generative model would have known the relationship between the structure and properties. A potential explanation is as follows: The QBM model acquires the latent features originating from a more generalized distribution, thus leading to a more appropriate distribution than the empirical distribution represented by the training dataset. Our results shed light on a new

approach with generative models beyond the variational inference leveraged by sampling from a quantum annealer.

Role of the Boltzmann Machine as a prior distribution

Most of the VAE models adopt a fixed distribution without learnable parameters such as the standard Gaussian distribution as the prior. The objective function of VAE tends to push the encoder to zero variance (*i.e.*, delta function), which thus leads to “posterior holes” in the latent space, thereby resulting in the low posterior probability and high prior probability³⁷. In the experiment, these holes are scattered in the wide region of the latent space rather than partitioned, and so the reconstruction from the holes generates bad samples³⁸. One possible solution to avoid them is to use a more flexible and trainable prior. Actually, in some reports the mixture of Gaussian with the trainable parameters was employed with respect to each component and coefficient of the prior³⁹. However, in most of these cases, the factorial Gaussian was applied for each component, where no correlation among the latent dimensions was postulated.

In this report, we adopted Quantum BM as a prior to resolve the afore-mentioned issues, which thereby extended the following two features: 1) BM naturally incorporates the correlation of the dimension via the coupler weights $\{J_{ij}\}$, and 2) the quantum annealer accelerates the extended sampling for the training of the correlation (Figure 3). Thus, the Quantum BM has a capability to effectively capture features of the data into its parameters and generates samples that improve the performance.

Perspectives on adaptation of quantum-driven generative models to drug discovery

The computer-aided molecular design technique is promising for efficiently finding novel candidates appropriate for pharmaceutical drugs. Our hybrid quantum-classical

generative models can generate molecules that are preferable in terms of the drug-likeness (QED score), even when compared to training datasets. Moreover, our hybrid quantum-classical generative models can also provide candidate molecules with significantly drastic structural changes (e.g. from chain to ring) in generated molecules, and thereby be utilized in searching for novel structures for us to intend the chemotype hopping, as discussed earlier (Figure 4).

In this manner, such quantum-driven generative models (machine/computer) provide us with candidates to significantly improve various properties related to drug-likeness through substantial modifications of the training dataset's chemical structures. Then, human beings (researchers/persons) can further modify the obtained molecular structures, which can comprise a new training dataset to be fed back into the quantum-driven generative models. Such a cyclical molecular-design process via computers and human beings, referred to here as computer-human cyclical molecular design, is a crucial and novel drug discovery process, thus leading to a dialogic interactive cooperation of quantum-driven generative AI models and human beings in the near future.

Conclusive remarks

We created a novel objective (loss) function that satisfies both differentiability and binarization for our quantum generative models. This loss function is free from both the mean-field approximation and assumptions of a type of stochastic distributions (notably, both of which are imposed in VAE), thus resulting in the improvement of outcomes derived from the VAE architecture. As a result of the analysis beyond VAE, the molecular properties of the obtained data generated by our present quantum generative models outperform even those of the training dataset. Thus, hybrid quantum and classical generative modeling is a promising technique in the near future of drug discovery field.

Methods

Training dataset

We used the subset of ChEMBL dataset provided by (Gircha, 2023)¹⁹ (<https://zenodo.org/records/7827952>). The compounds are divided into training, validation, and test sets by 8:1:1 (128,800 for training, 15,360 for validation, and 15,360 for test sets). The canonical SMILES strings are obtained from the molecular structures of the dataset.

Autoencoder

We employed the encoder-decoder architecture of Transformer²⁸ for featurizing and recomposing the SMILES strings (Figure 1). Each token from SMILES is embedded in a 160-dimensional vector and positional encoding was added. The embedded tensors are fed into the Transformer encoder layers and flattened by the Neural Tensor Network layer (see the Neural Tensor Network part in Methods section for details) to obtain the fixed-length vectors for the latent variables. In the decoder block, the input tensors are passed through the self-attention layer with the subsequent masks. The cross-attention between the output of the self-attention layer and the latent variables were transformed by another Neural Tensor Network layer. Finally, SMILES sequences are reconstructed from outputs of the decoder through the softmax layer. In the generation phase, the latent variables sampled from the prior distribution are fed into the Neural Tensor Network and decoder, and the output tokens are predicted by the auto-regressive manner.

Boltzmann machine as a prior

Whereas priors are conventionally fixed to a standard Gaussian distribution, we parameterize the prior with Boltzmann machine (BM)-based distribution powered by the

quantum annealer. The BM⁴⁰ can learn a complex multi-modal probability distribution and is thus an attractive approach for integrating quantum computing into deep generative models.

The probability distribution of the BM is

$$p_\psi(z) = \frac{\exp(-\beta E_\psi(z))}{Z_\psi}, \quad Z_\psi = \sum_z \exp(-\beta E_\psi(z))$$

$$E_\psi(z) = \sum_{i < j} J_{ij} z_i z_j + \sum_{i=1}^d h_i z_i, \quad (7)$$

where $z \in \{-1, 1\}^d$ is the binary latent variables, β is the inverse temperature parameter, and Z_ψ is the partition function. $\psi = \{J, h\}$ are the trainable parameters: J_{ij} denotes the interaction coefficients between unit i and j , and h_i denotes the bias term. The Restricted Boltzmann Machine (RBM) is a subtype of BM, widely used because of its efficient training⁴¹. In the RBM, a latent variable is divided into the visible units $v = \{v_i\}_{i=1}^{d_v}$ and hidden units $h = \{h_i\}_{i=1}^{d_h}$, where the interactions are limited to between visible and hidden units.

We considered another BM formulation wherein the visible units form interactions, similar to the Semi-restricted Boltzmann Machine⁴². The Hamiltonian is defined as

$$E_\psi(v, h) = \sum_{i < j} J_{ij} v_i v_j + \sum_{i=1}^{d_v} \sum_{k=1}^{d_h} L_{ik} v_i h_k + \sum_{i=1}^{d_v} b_i v_i + \sum_{k=1}^{d_h} c_k h_k. \quad (8)$$

Since the hidden units remain independent, the conditional distribution of the hidden units can be calculated independently by

$$p(h_k|v) = \tanh(h_k \lambda_k(v)), \quad \lambda_k(v) = c_k + \sum_i L_{ik} v_i. \quad (9)$$

We applied the distribution marginalized over the hidden units

$$p_\psi(v) = \frac{\sum_h \exp(-\beta E_\psi(v, h))}{Z_\psi}, \quad (10)$$

to the prior distribution. Therefore, the KL-divergence term of the objective function is given by

$$D_{KL}(q_\phi(\zeta|x) \mid\mid p_\psi(\zeta)) = \mathbb{E}_{q_\phi}[\log q_\phi(\zeta)] - \mathbb{E}_{q_\phi}[\log p_\psi(\zeta)], \quad (11)$$

and the gradient of the second term is calculated by the difference of energy between samples from the data (positive phase) and from the prior (negative phase) as

$$\begin{aligned} \mathbb{E}_{q_\phi}[\partial \log p_\psi(\zeta)] &= \mathbb{E}_{\zeta \sim q_\phi}[\partial F_\psi(\zeta)] - \mathbb{E}_{v, h \sim p_\psi(v, h)}[\partial E_\psi(v, h)] \\ F_\psi(\zeta) &= \sum_{i < j} J_{ij} \zeta_i \zeta_j + \sum_i b_i \zeta_i - \sum_k \log 2 \cosh(-\lambda_k(\zeta)), \end{aligned} \quad (12)$$

where F_ψ is the marginalized Hamiltonian (free energy) of visible units. This equation means that the first term is calculated by the average of the latent variables from the data and the second term is calculated using samples from the prior distribution. We used simulated annealing with Metropolis-Hastings update to approximate sampling from BM.

Quantum Boltzmann machine and its implementation

We use the D-Wave quantum annealer as a source of prior samples. When the annealing time is sufficiently long with quasistatic evolution, the quantum processing unit (QPU) generates samples that approximate a classical Boltzmann distribution⁴³. However, the presence of a finite transverse field introduces quantum fluctuations that can lead to deviations from the ideal Boltzmann statistics. A quantum Boltzmann machine (QBM)²¹, which draws samples from the Boltzmann distribution of a transverse-field Ising Hamiltonian,

can be trained analogously to its classical counterpart by optimizing a variational bound on the true log-likelihood. In this study, we introduce an RBM architecture that is restricted to the Zephyr graph (*i.e.*, an architecture native to the D-Wave QPU), thus allowing for more efficient sampling and larger dimensions than a traditional architecture, such as bipartite and clique graphs, which are not native to the Zephyr graph. In this study, the largest possible clique and bipartite graphs that could be built on a defect-free Zephyr architecture are $K_{2(2m-1)t}$ and $K_{2(2m-1)t,2(2m-1)t}$, respectively, where m is the grid parameter and t is the tile parameter⁴⁴. The QPU used in this study has a grid parameter of 6 and a tile parameter of 4, only allowing a clique of 88 and a $K_{88,88}$ (*i.e.*, a bipartite graph with 88 units on the visible side and 88 units on the hidden side).

To utilize the entire QPU as an RBM prior and allow for a flexible number of visible and hidden units, we use chains of qubits to achieve the desired prior dimension as well as increase the connectivity between visible units. The choice of chains and hidden nodes is defined through a heuristic node-contraction method where a sparse graph is iteratively converted to a denser graph, starting with a chain length of two and increasing the length as needed. In this method, nodes are first sorted by degree. The node with the lowest degree along with its adjacent nodes, which also have the smallest degree, are chosen for contraction. When the resulting contracted graph reaches the required dimensions, the contraction stops. The node-contraction method works with any graph and especially with D-Wave's current and future quantum annealing architectures. One advantage of this method is that it works with QPUs with imperfect graphs and allows for a granular control over the number of visible and hidden variables. In our implementation of the Boltzmann machine, the hidden units are not connected to each other, which is compatible with the Zephyr graph as there are groups of qubits that are not connected to each other. Figure S1 (see Supporting Information) illustrates the classification of qubits within the Zephyr architecture into four distinct groups, referred to

as color groups. Color groups are suitable candidates for hidden units, because a color group does not have any internal connections, whereas different color groups have external connections between each other. In the Advantage2_prototype2.6 QPU, each color group contains more than 300 qubits and all hidden units are selected exclusively from a single-color group to ensure compliance with the no-connectivity constraint among hidden units; that is, selecting hidden variables from multiple color groups would violate this constraint. If the number of hidden units were to exceed 300, couplers would need to be removed to adhere to the no-connectivity condition between hidden units; however, 300 hidden units are deemed sufficient for the scope of this study. Figure S2 (see Supporting Information) shows a Zephyr graph that we used as an RBM prior, having 128 visible and 128 hidden units. Note that we utilized the entire QPU (1215 qubits) in this prior, where chains were added to increase the connectivity of visible units.

When sampling from the QPU, one may need to know the effective temperature (β) at which sampling is performed. We could estimate this temperature using the maximum log-likelihood approach based on the model parameters and rate of excitations ⁴⁵, which are available with a D-Wave utility

(https://docs.ocean.dwavesys.com/en/latest/docs_system/reference/generated/dwave.system.temperatures.maximum_pseudolikelihood_temperature.html). In this study, we scale J and b parameters of the Hamiltonian such that the QPU produces samples with an effective temperature near 1.0.

Neural Tensor Network

A compound in the training data is embedded to tensor $x \in \mathbb{R}^{C \times d_{model}}$, where C is the number of token sequences and d_{model} is the embedding dimension. Since the sequence length varies for each compound, the tensor size is also variable. To obtain the latent vector

with fixed length, it is necessary to convert the variable length tensor to the fixed length one. The simplest way is to aggregate the vectors of each length by the pooling (max, average, etc.). However, this can cause information loss concerning the length. Another method is convolution/deconvolution for converting to the fixed length vector, wherein the range of the length is fixed in advance for determining the strides. We propose a more flexible form, which is referred to here as Neural Tensor Network (NTN), using tensor products with trainable higher-order tensors. For the end of the encoder (NTN1) (Figure 1), conversion from the variable length tensor x to fixed length vector $h \in \mathbb{R}^D$ is performed as follows:

$$b_\alpha = \sum_{i=1}^d \sum_{j=1}^d \sum_{k=1}^n W_{ij\alpha}^{(1)} x_{ki} x_{kj}, \quad h_\alpha = \sigma(b_\alpha), \quad (13)$$

where $\mathcal{W}^{(1)} = \{W_{ij\alpha}^{(1)}\} \in \mathbb{R}^{d_{model} \times d_{model} \times D}$ is a trainable tensor and $\sigma(\cdot)$ is an element-wise activation function. For the beginning of the decoder (NTN2) (Figure 1), conversion from the latent vector $\zeta \in \mathbb{R}^D$ to the tensor $M \in \mathbb{R}^{m \times d}$ is performed as follows:

$$B_{li} = \sum_{\alpha=1}^D W_{\alpha li}^{(2)} \zeta_\alpha, \quad M_{li} = \sigma(B_{li}), \quad (14)$$

where $\mathcal{W}^{(2)} = \{W_{\alpha li}^{(2)}\} \in \mathbb{R}^{D \times m \times d}$ is a trainable tensor.

Derivation of the gradient of NHF with respect to the encoder parameters

Using chain rules, the gradient of the loss in Neural Hash Function L_{nhf} (Equation 5) with respect to ϕ is

$$(15)$$

$$= \sum_n^N \left(\frac{\partial L_{rec}}{\partial z_n} + \frac{\partial L_{prior}}{\partial z_n} + \frac{\partial L_{quant}}{\partial z_n} \right) \frac{\partial z_n}{\partial h_n} \frac{\partial h_n}{\partial \phi}.$$

Using vector-form, L_{quant} can be rewritten as

$$\begin{aligned} L_{quant} &= \frac{\lambda_{fro}}{2N} \|Z - H\|_F^2 + \frac{\lambda_{ortho}}{2} \sum_l \|W_l W_l^T - I\|_F^2 \\ &= \frac{\lambda_{fro}}{2N} \sum_n \|z_n - h_n\|^2 + \frac{\lambda_{ortho}}{2} \sum_l \|W_l W_l^T - I\|_F^2 \end{aligned} \quad (16)$$

and the gradient of L_{quant} with respect to z_n are computed to

$$\frac{\partial L_{quant}}{\partial z_n} = \frac{\lambda_{fro}}{N} (z_n - h_n). \quad (17)$$

When the transformation from h_n to z_n is non-smooth, such as the Sign function or Heaviside step function, the gradient $\frac{\partial z_n}{\partial h_n}$ cannot be computed. We approximated this derivative by the identity function. With this approximation, the backward pass is different from the forward pass; whereas the sign of negation of the backward pass is consistent with the direction that minimizes the loss^{33,46}. From Equations 15 and 17, we obtained

$$\frac{\partial L_{nhf}}{\partial \phi} = \sum_n^N \left(\frac{\lambda_{fro}}{N} (z_n - h_n) + \frac{\partial L_{prior}}{\partial z_n} + \frac{\partial L_{rec}}{\partial z_n} \right) \frac{\partial h_n}{\partial \phi}. \quad (18)$$

Relationships between transformation of chemical structures and improvements of QED score

We selected the representative compounds from the training data using the following criteria: 1) Molecular Weight (MW) > 200 and < 450, 2) $0 < \log P < 4$, 3) PSA < 150, and 4) without alert structures (computed by RDKit). As queries of substructure search, a pool of

fragments from the representative compounds was created using RECAP⁴⁷ and BRICS⁴⁸ fragmentation and filtered by MW (> 150). From the generated compounds, we extracted those that shared the same substructures as those of each of representative compounds. Herein, for a similarity measure, the Matching Coefficient (MC) of atoms was computed as follows

$$MC = \frac{HAC_{matched}}{HAC_{generated} + HAC_{train} - HAC_{matched}}, \quad (19)$$

where $HAC_{generated}$, HAC_{train} , and $HAC_{matched}$ denote the Heavy Atom Count (HAC) of the generated compound, the training data, and the matched substructure, respectively. For another similarity measure, we used the Tanimoto Similarity of the molecular fingerprint. Molecular fingerprints are generated as 2048-bit vectors using Morgan algorithm⁴⁹ with radius of 2, which is roughly equivalent to ECFP4 fingerprint⁵⁰.

Data Availability

In the current study, we used the subset of ChEMBL dataset provided by the previous report¹⁹ (<https://doi.org/10.5281/zenodo.7827952>). The code and the generated molecules during the current study are available from the corresponding author on reasonable request.

References

1. Bohacek, R. S., McMardin, C. & Guida, W. C. The art and practice of structure-based drug design: a molecular modeling perspective. *Medicinal research reviews* **16**, 3–50 (1996).
2. Ajagekar, A. & You, F. Molecular design with automated quantum computing-based deep learning and optimization. *npj Computational Materials* **9**, 143 (2023).
3. Dollar, O., Joshi, N., Beck, D. A. & Pfaendtner, J. Attention-based generative models for

de novo molecular design. *Chemical Science* **12**, 8362–8372 (2021).

4. Lambrinidis, G. & Tsantili-Kakoulidou, A. Challenges with multi-objective QSAR in drug discovery. *Expert Opinion on Drug Discovery* **13**, 851–859 (2018).
5. Sadybekov, A. A. *et al.* Synthon-based ligand discovery in virtual libraries of over 11 billion compounds. *Nature* **601**, 452–459 (2022).
6. Devadas, R. M. & Sowmya, T. Quantum machine learning: A comprehensive review of integrating AI with quantum computing for computational advancements. *MethodsX* 103318 (2025) doi:<https://doi.org/10.1016/j.mex.2025.103318>.
7. McClean, J. R., Boixo, S., Smelyanskiy, V. N., Babbush, R. & Neven, H. Barren plateaus in quantum neural network training landscapes. *Nat Commun* **9**, 4812 (2018).
8. Cerezo, M. *et al.* Does provable absence of barren plateaus imply classical simulability? *Nat Commun* **16**, 7907 (2025).
9. Albash, T. & Lidar, D. A. Adiabatic quantum computation. *Rev. Mod. Phys.* **90**, 015002 (2018).
10. Johnson, M. W. *et al.* Quantum annealing with manufactured spins. *Nature* **473**, 194–198 (2011).
11. Amin, M. H., Andriyash, E., Rolfe, J., Kulchytskyy, B. & Melko, R. Quantum Boltzmann Machine. *Phys. Rev. X* **8**, 021050 (2018).
12. Benedetti, M., Realpe-Gómez, J., Biswas, R. & Perdomo-Ortiz, A. Quantum-Assisted Learning of Hardware-Embedded Probabilistic Graphical Models. *Phys. Rev. X* **7**, 041052 (2017).
13. Winci, W. *et al.* A path towards quantum advantage in training deep generative models with quantum annealers. *Mach. Learn.: Sci. Technol.* **1**, 045028 (2020).
14. King, A. D. *et al.* Quantum critical dynamics in a 5,000-qubit programmable spin glass. *Nature* **617**, 61–66 (2023).

15. King, A. D. *et al.* Beyond-classical computation in quantum simulation. *Science* **388**, 199–204 (2025).
16. Kingma, D. P. & Welling, M. Auto-encoding variational bayes. *arXiv preprint arXiv:1312.6114* (2013).
17. Rezende, D. J., Mohamed, S. & Wierstra, D. Stochastic backpropagation and approximate inference in deep generative models. in *International conference on machine learning* 1278–1286 (PMLR, 2014). doi:<https://doi.org/10.48550/arXiv.1401.4082>.
18. Rolfe, J. T. Discrete variational autoencoders. *arXiv preprint arXiv:1609.02200* (2016).
19. Gircha, A. I., Boev, A. S., Avchaciov, K., Fedichev, P. O. & Fedorov, A. K. Hybrid quantum-classical machine learning for generative chemistry and drug design. *Scientific Reports* **13**, 8250 (2023).
20. Khoshaman, A. *et al.* Quantum variational autoencoder. *Quantum Science and Technology* **4**, 014001 (2018).
21. Amin, M. H., Andriyash, E., Rolfe, J., Kulchytskyy, B. & Melko, R. Quantum Boltzmann machine. *Physical Review X* **8**, 021050 (2018).
22. Khoshaman, A. H. & Amin, M. Gumbolt: Extending Gumbel trick to Boltzmann priors. in *Advances in Neural Information Processing Systems* vol. 31 (2018).
23. Erin Liong, V., Lu, J., Wang, G., Moulin, P. & Zhou, J. Deep hashing for compact binary codes learning. in *Proceedings of the IEEE Conference on Computer Vision and Pattern Recognition* 2475–2483 (2015). doi:<https://doi.org/10.1109/CVPR.2015.7298862>.
24. Weininger, D. SMILES, a chemical language and information system. 1. Introduction to methodology and encoding rules. *J. Chem. Inf. Comput. Sci.* **28**, 31–36 (1988).
25. Krenn, M. *et al.* SELFIES and the future of molecular string representations. *Patterns* **3**, 100588 (2022).
26. Winci, W. *et al.* A path towards quantum advantage in training deep generative models with

quantum annealers. *Machine Learning: Science and Technology* **1**, 045028 (2020).

27. Maddison, C. J., Mnih, A. & Teh, Y. W. The concrete distribution: A continuous relaxation of discrete random variables. *arXiv preprint arXiv:1611.00712* <https://doi.org/10.48550/arXiv.1611.00712> (2016)
doi:<https://doi.org/10.48550/arXiv.1611.00712>.

28. Vaswani, A. *et al.* Attention is all you need. in *Advances in Neural Information Processing Systems* vol. 30 (2017).

29. Bickerton, G. R., Paolini, G. V., Besnard, J., Muresan, S. & Hopkins, A. L. Quantifying the chemical beauty of drugs. *Nature Chemistry* **4**, 90–98 (2012).

30. Higgins, I. *et al.* beta-vae: Learning basic visual concepts with a constrained variational framework. in *International conference on learning representations* (2017).

31. Tolstikhin, I., Bousquet, O., Gelly, S. & Schoelkopf, B. Wasserstein auto-encoders. *arXiv preprint arXiv:1711.01558* <https://doi.org/10.48550/arXiv.1711.01558> (2017)
doi:<https://doi.org/10.48550/arXiv.1711.01558>.

32. Zhao, S., Song, J. & Ermon, S. Infovae: Information maximizing variational autoencoders. *arXiv preprint arXiv:1706.02262* <https://doi.org/10.48550/arXiv.1706.02262> (2017)
doi:<https://doi.org/10.48550/arXiv.1706.02262>.

33. Yin, P. *et al.* Understanding straight-through estimator in training activation quantized neural nets. *arXiv preprint arXiv:1903.05662* (2019).

34. Hoffman, M. D. & Johnson, M. J. Elbo surgery: yet another way to carve up the variational evidence lower bound. in *Workshop in Advances in Approximate Bayesian Inference, NIPS* vol. 1 (2016).

35. Bowman, S. *et al.* Generating sentences from a continuous space. in *Proceedings of the 20th SIGNLL conference on computational natural language learning* 10–21 (2016).
doi:<https://doi.org/10.48550/arXiv.1511.06349>.

36. Serban, I. *et al.* A hierarchical latent variable encoder-decoder model for generating dialogues. in *Proceedings of the AAAI conference on artificial intelligence* vol. 31 (2017).

37. Rezende, D. J. & Viola, F. Taming VAEs. Preprint at <https://doi.org/10.48550/ARXIV.1810.00597> (2018).

38. Rosca, M., Lakshminarayanan, B. & Mohamed, S. Distribution Matching in Variational Inference. Preprint at <https://doi.org/10.48550/ARXIV.1802.06847> (2018).

39. Tomczak, J. & Welling, M. VAE with a VampPrior. in *Proceedings of the Twenty-First International Conference on Artificial Intelligence and Statistics* (eds Storkey, A. & Perez-Cruz, F.) vol. 84 1214–1223 (PMLR, 2018).

40. Ackley, D. H., Hinton, G. E. & Sejnowski, T. J. A learning algorithm for Boltzmann machines. *Cognitive Science* **9**, 147–169 (1985).

41. Hinton, G. E., Osindero, S. & Teh, Y. W. A fast learning algorithm for deep belief nets. *Neural Computation* **18**, 1527–1554 (2006).

42. Osindero, S. & Hinton, G. E. Modeling image patches with a directed hierarchy of Markov random fields. in *Advances in Neural Information Processing Systems* vol. 20 (2007).

43. Amin, M. H. Searching for quantum speedup in quasistatic quantum annealers. *Physical Review A* **92**, 052323 (2015).

44. Boothby, K., King, A. D. & Raymond, J. *Zephyr Topology of D-Wave Quantum Processors*. https://www.dwavesys.com/media/2uznec4s/14-1056a-a_zephyr_topology_of_d-wave_quantum_processors.pdf (2021).

45. Raymond, J., Yarkoni, S. & Andriyash, E. Global warming: Temperature estimation in annealers. *Frontiers in ICT* **3**, 23 (2016).

46. Hinton, G. Neural networks for machine learning. in (Coursera, 2012).

47. Lewell, X. Q., Judd, D. B., Watson, S. P. & Hann, M. M. RECAPRetrosynthetic Combinatorial Analysis Procedure: A Powerful New Technique for Identifying Privileged

Molecular Fragments with Useful Applications in Combinatorial Chemistry. *J. Chem. Inf. Comput. Sci.* **38**, 511–522 (1998).

48. Degen, J., Wegscheid-Gerlach, C., Zaliani, A. & Rarey, M. On the Art of Compiling and Using ‘Drug-Like’ Chemical Fragment Spaces. *ChemMedChem* **3**, 1503–1507 (2008).

49. Morgan, H. L. The Generation of a Unique Machine Description for Chemical Structures—A Technique Developed at Chemical Abstracts Service. *J. Chem. Doc.* **5**, 107–113 (1965).

50. Rogers, D. & Hahn, M. Extended-Connectivity Fingerprints. *J. Chem. Inf. Model.* **50**, 742–754 (2010).

Acknowledgements

This study received no funding.

Author contributions

H.K., M.R. Y.I., V.V.C., W.K., K.C., M.A. and M.T. designed research. H.K., Y.I., Y.H., A.S. and M.T. constructed the generative models, ran experiments and analyzed the data. M.R., M.W., V.V.C., W.K., K.C. and M.A. contributed to implementation of the quantum annealing. All the authors discussed the results and contributed to writing the manuscript.

Competing interests

The authors have no competing interests.

Tables

Table 1. Metrics of compounds generated by Transformer-based encoder-decoder models.

Sampler	Binarization	Validity (%)	Uniqueness (%)	Unique compounds / generated compounds
Classical BM	Gumbel-Softmax	52.20	<u>99.94</u>	5216 / 10000
	NHF	61.95	98.09	6077 / 10000
QBM	Gumbel-Softmax	71.88	95.10	<u>6835 / 10000</u>
	NHF	<u>96.97</u>	51.92	5035 / 10000

Validity is a fraction of the SMILES sequences that can be interpreted to the molecular graph by employing RDkit. Uniqueness is a fraction of compounds that are uniquely (not redundantly) found in the valid compounds.

Table 2. Drug-likeness of generated compounds by Transformer-based encoder-decoder models.

Data	Sampler	Binarization	Drug-like compounds (%)
Training data			0.316
Generated samples	Classical BM	Gumbel-Softmax	0.408
	QBM	Gumbel-Softmax	0.523
		NHF	<u>0.668</u>

We defined the drug-like compounds as those with the QED score of 0.7 or higher and showed the drug-like compounds as a proportion of unique compounds.

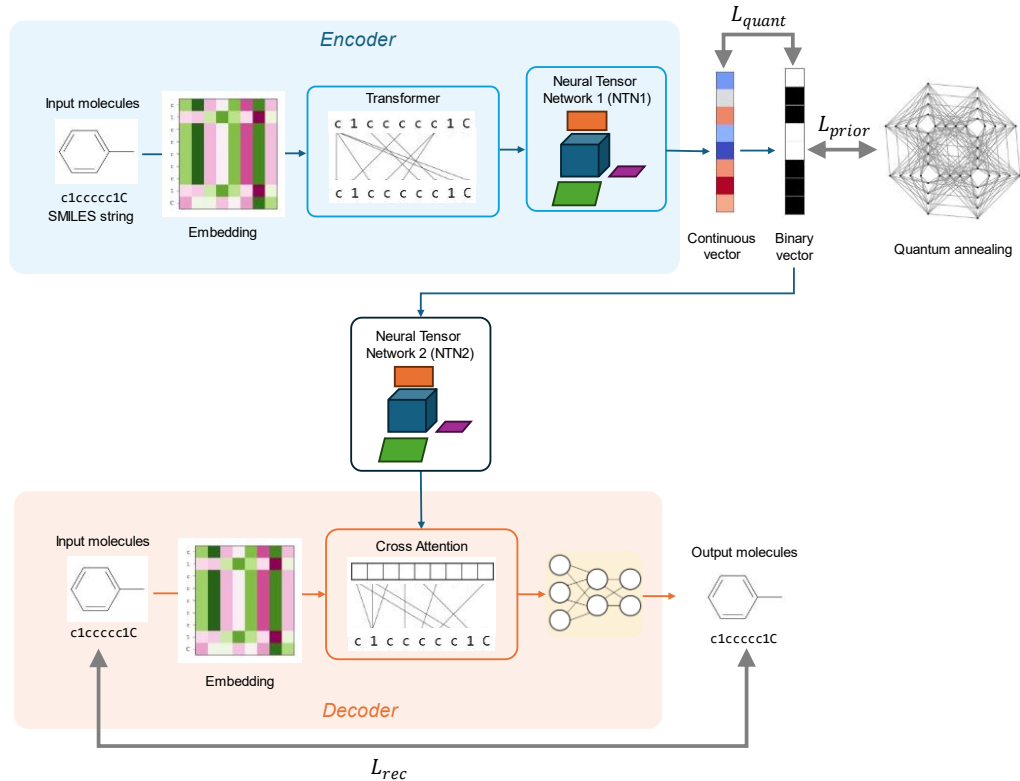
Table 3. Metrics of compounds generated by MLP-based encoder-decoder models.

Sampler	Binarization	Validity (%)	Uniqueness (%)	Unique compounds / generated compounds
Classical BM	Gumbel-Softmax	38.50	<u>100.00</u>	3848 / 10000
	NHF	58.30	74.90	4367 / 10000
QBM	Gumbel-Softmax	39.30	<u>100.00</u>	3929 / 10000
	NHF	<u>59.90</u>	86.30	<u>5198 / 10000</u>

Definitions of validity and uniqueness are identical to those of Table 1.

Figures

a) Training phase



b) Generation phase

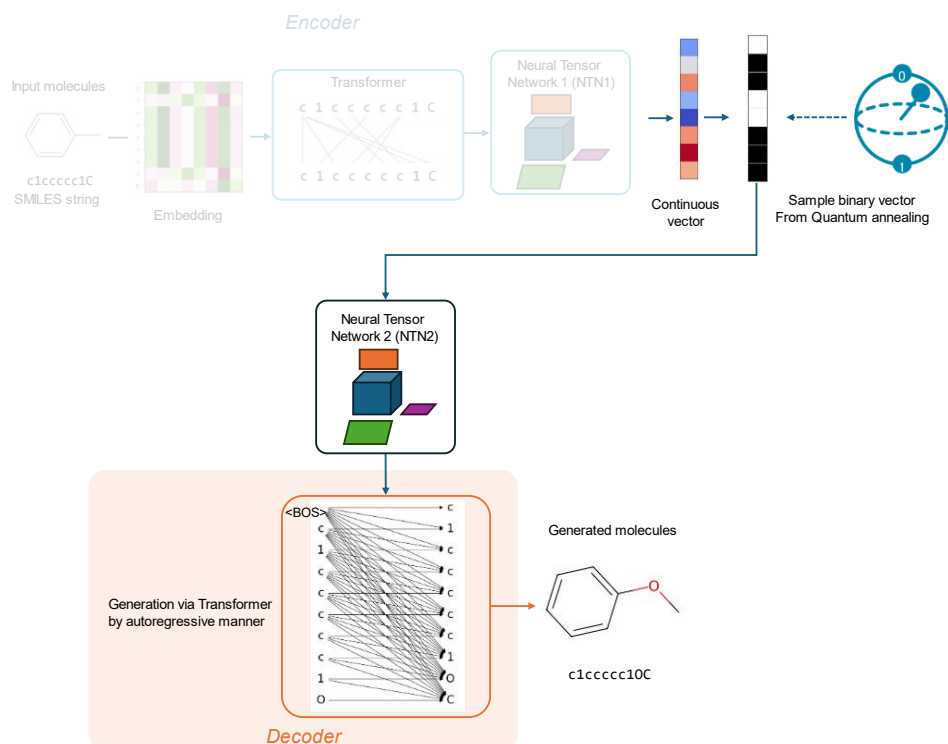


Figure 1. Scheme of the Neural Hash Function (NHF)-based generative model.

(a) Input compound X is represented by employing SMILES sequences. Each token from SMILES is embedded in a 160-dimensional vector and added the positional encoding. The embedded tensor is fed into the Transformer encoder layers and flattened by the Neural Tensor Network layer (NTN1) to obtain the continuous vector h . h is transformed by our NHF to the binary vector z , and then transformed into the latent matrix through another NTN layer (NTN2). In decoder block, the input tensors are passed through the self-attention layer with the subsequent masks. The cross-attention between the output of the self-attention layer and the latent matrix. Finally, SMILES sequences are reconstructed from outputs of the decoder through the softmax layer. The reconstruction loss between the input and reconstructed tokens (L_{rec}), the cross entropy of the prior distribution (L_{prior}) and the quantization loss to produce good binary codes (L_{quant}) are computed for updating of parameters of the encoder, decoder and prior (see Equation 5).

(b) In the generation phase, the binary latent variables are sampled from the Quantum or classical Boltzmann Machine (BM) prior, and transformed into the latent matrix through the NTN2. The output SMILES sequences are predicted by autoregressive manner.

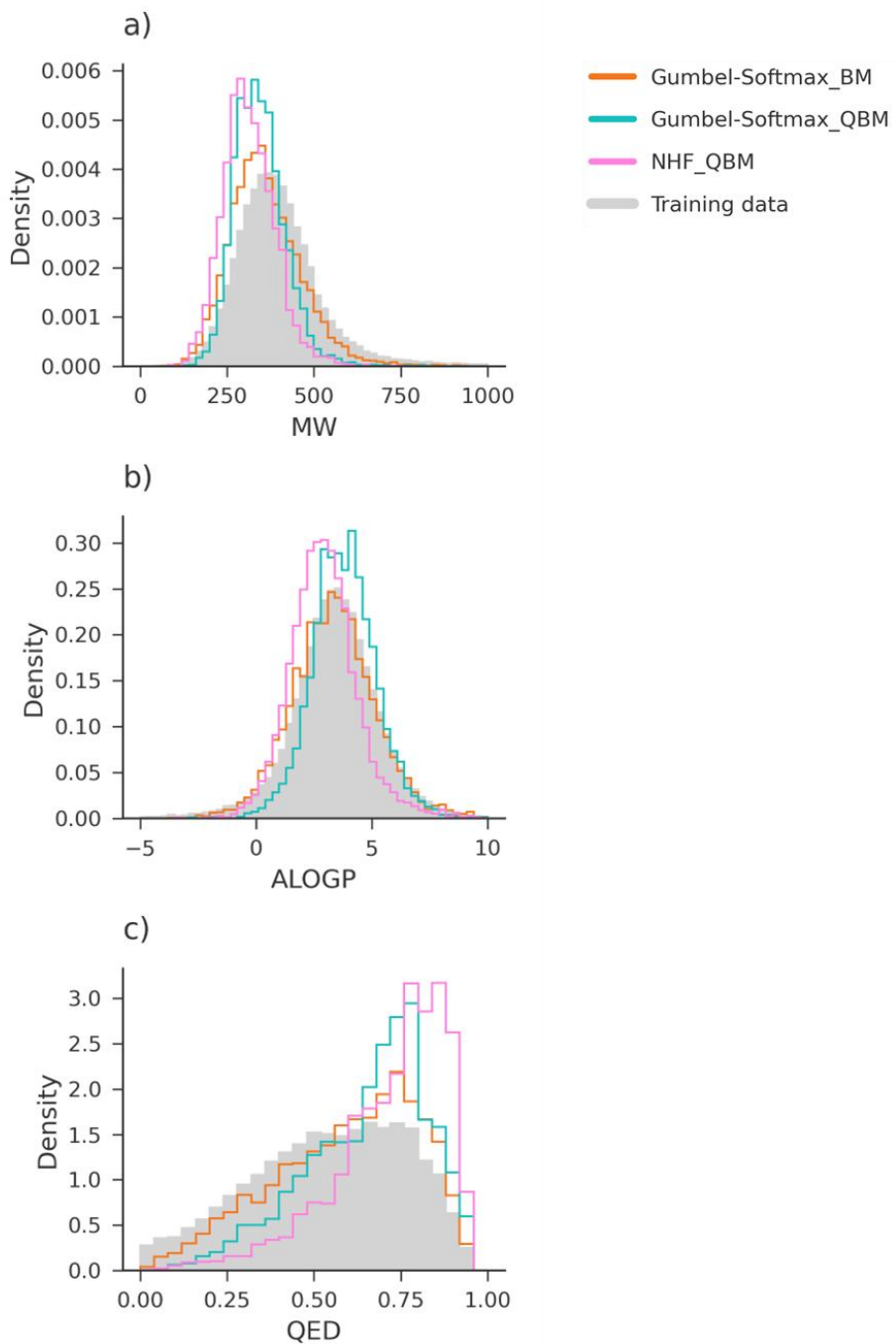


Figure 2. Distributions of various molecular properties of generated compounds.

Three properties are shown: molecular weight (MW), lipophilicity (ALOGP), and drug-likeness score (QED). All of these properties were calculated by employing RDkit. Gray bars denote the training dataset, and orange, cyan and pink lines denote the samples from the Gumbel -Softmax with classical BM, the Gumbel-Softmax with QBM and the NHF with QBM, respectively.

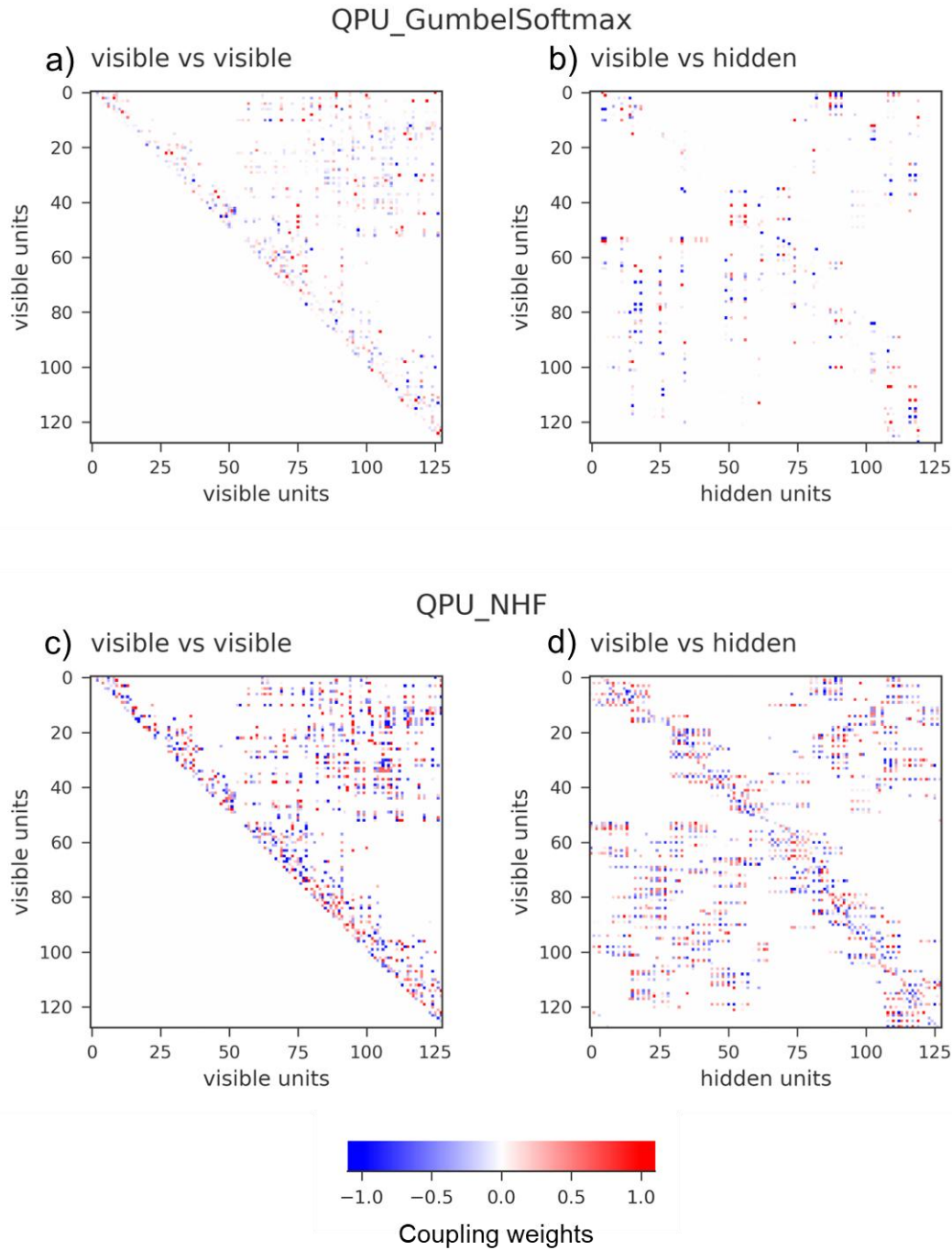


Figure 3. Coupling weights of the Ising Hamiltonian trained in the generative models.

(a)-(b) Heatmaps of the coupling weights between visible and visible units ($\{J_{ij}\}$ in Equation 8; a) and between visible and hidden units ($\{L_{ik}\}$ in Equation 8; b) of Gumbel-Softmax-based model with QPU. Note that J is the upper-triangular matrix and there are no interactions between hidden units.

(c)-(d) Heatmaps of the coupling weights of NHF-based model with QPU.

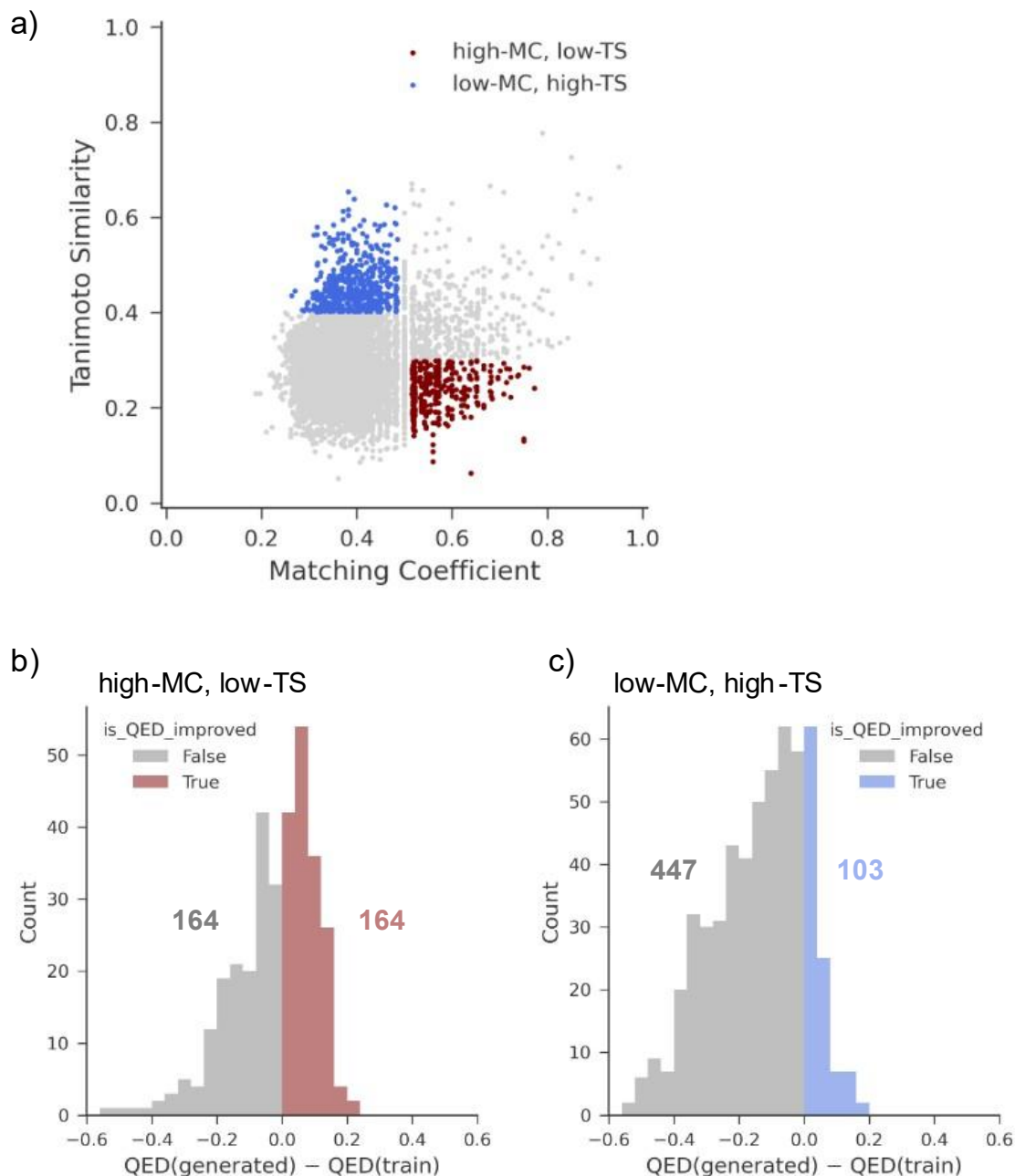


Figure 4. Relationships between structural transformation and QED improvements from QBM models.

(a) The scatter plot of Matching Coefficient (MC) and Tanimoto Similarity (TS) with respect to the subset of generated compounds, that was selected from the QBM model so as for substructures of generated compounds to be matched with those of the training data, as described in the main text (see Results and Method sections). The red and blue points denote the regions with high MC and low TS ($MC > 0.5$ and $TS < 0.2$), and low MC and high TS ($MC < 0.5$ and $TS > 0.4$), respectively (see Methods for detail).

(b)-(c) Differences of the QED score between the generated and original (matched) compounds in the generated and training data, respectively. In the subset of compounds, the features are defined by a) “is_QED_improved”, which means that the difference of the QED score is larger than zero. The numbers in the histograms denote those of compounds that exhibit improved QED score values (red in (b) or blue in (c)) and not improved QED (gray), respectively.

Supplementary Information

Molecular Design beyond Training Data with Novel Extended Objective Functionals of Generative AI Models Driven by Quantum Annealing Computer

Hayato Kunugi¹, Mohsen Rahmani², Yosuke Iyama¹, Yutaro Hirono¹, Akira Suma¹, Matthew Woolway², Vladimir Vargas-Calderón², William Kim², Kevin Chern², Mohammad Amin², and Masaru Tateno^{1*}

1 Innovation to Implementation Laboratories, Central Pharmaceutical Research Institute, Japan Tobacco Inc., Takatsuki, Osaka 569-1125, Japan

2 D-Wave Systems Inc., 3033 Beta Ave, Burnaby, BC V5G 4M9, Canada

* Corresponding should be addressed.

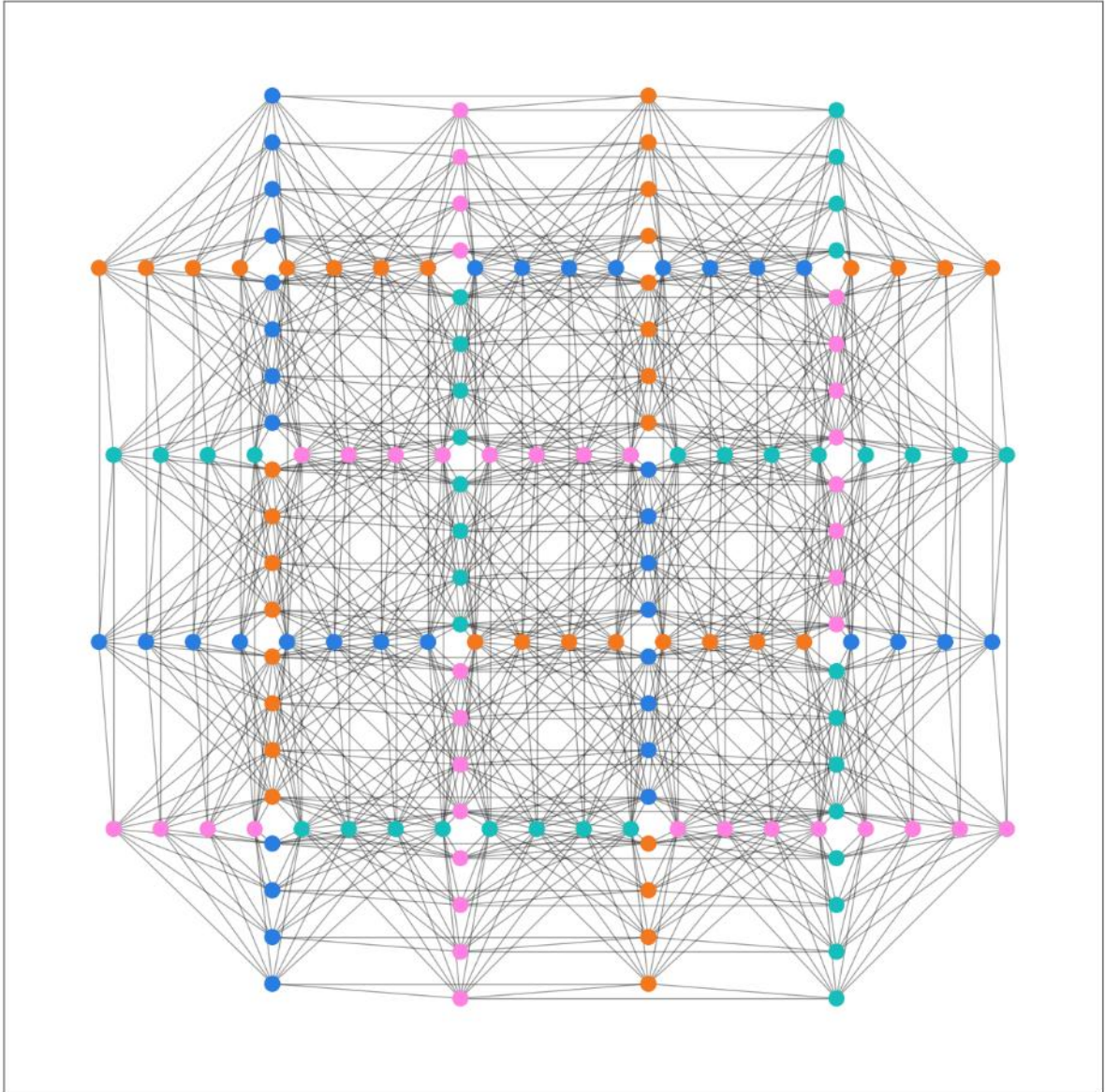


Figure S1. Zephyr structure consisting of 4 color groups.

Qubits and their connections are illustrated by a graph structure. The qubits are classified into four distinct groups referred to as color groups. Since a color group does not have any internal connections, we assign one of color groups to hidden units that remain independent and the other groups to visible units (Equation 7).

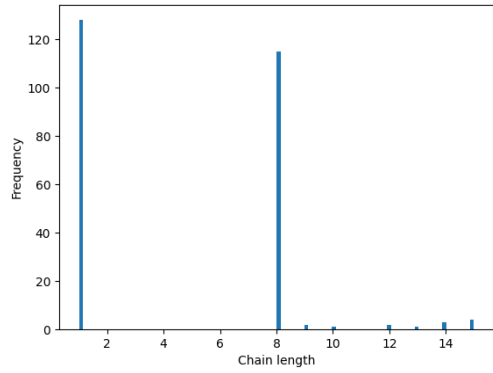
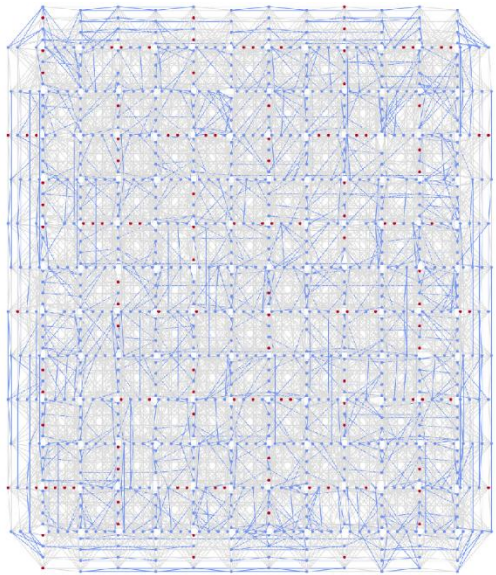


Figure S2. RBM structure used for training, with a histogram of chain lengths.

(Left) RBM structure used for training, possessing 128 visible units and 128 hidden units, where the red dots are hidden units, blue dots are visible units, blue lines are chain couplers between visible units, and gray lines are couplers between units. (Right) Histogram of chain lengths. Long chains are created with the maximum number of qubits being 1215, where the desired graph is required to have 256 logical qubits.

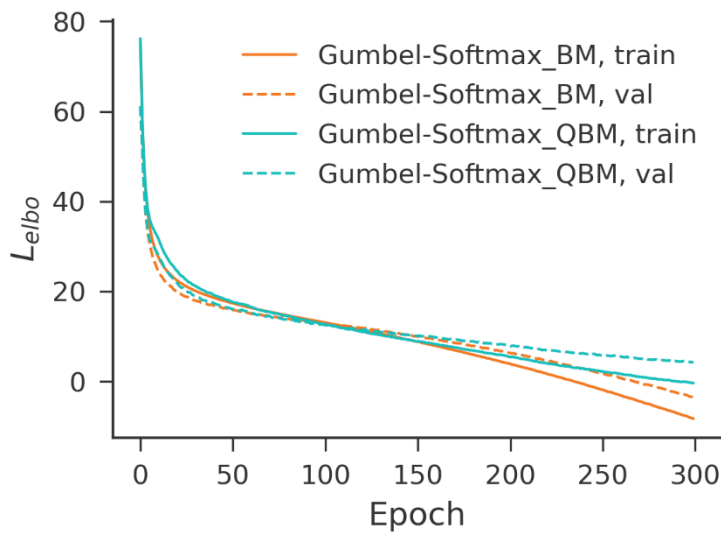


Figure S3.

Solid and dashed lines denote the training and validation loss (Equation 3). Orange and cyan lines denote the samples from classical BM and QBM in DVAE, respectively.